Determination of the basic optical parameters of $ZnSnN_2$

Fuling Deng,[1,2] Hongtao Cao,[2] Lingyan Liang,[2,*] Jun Li,[2] Junhua Gao,[2] Hongliang Zhang,[2] Ruifeng Qin,[2] and Caichi Liu[1,3]

[1]*School of Materials Science and Engineering, Hebei University of Technology (HEBUT), Tianjin 300401, China*

[2]*Division of Functional Materials and Nano Devices, Ningbo Institute of Materials Technology and Engineering (NIMTE), Chinese Academy of Sciences (CAS), Ningbo 315201, China*

[3]*e-mail: ccliu@hebut.edu.cn*

**Corresponding author: lly@nimte.ac.cn*

Received December 10, 2014; revised February 15, 2015; accepted February 16, 2015; posted February 18, 2015 (Doc. ID 229103); published March 20, 2015

Polycrystalline $ZnSnN_2$ thin films were successfully prepared by DC magnetron sputtering at room temperature. Both the as-deposited and annealed films showed n-type conduction, with electron concentration varying between 1.6×10^{18} and 2.3×10^{17} cm^{-3} and the maximum mobility of 3.98 cm^2 V^{-1} s^{-1}. The basic optical parameters such as the refraction index, extinction coefficient, and absorption coefficient were precisely determined through the spectroscopic ellipsometry measurement and analysis. The optical bandgap of the $ZnSnN_2$ films was calculated to around 1.9 eV, with the absorption coefficient greater than 10^4 cm^{-1} at wavelengths less than 845 nm. The easy-fabricated $ZnSnN_2$ possesses a sound absorption coefficient ranging from the ultraviolet through visible light and into the near-infrared, comparable to some typical photovoltaic materials such as GaAs, CdTe, and InP.

OCIS codes: (160.2100) Electro-optical materials; (040.5350) Photovoltaic; (310.6860) Thin films, optical properties; (300.6560) Spectroscopy, x-ray; (300.1030) Absorption.

http://dx.doi.org/10.1364/OL.40.001282

Thin-film solar cell (TFSC) technique, as an efficient, cost-effective approach to directly convert sunlight into electricity, has considerably matured over the last several decades. At present, in view of the material cost and environmental impact, the Earth-abundance and nontoxicity of photovoltaic film materials is a critical issue for large-scale (terawatt-level) photovoltaic power generation by TFSCs [1,2]. Meanwhile, low-temperature deposition techniques can facilitate the manufacture of TFSCs on flexible substrates such as plastics, paper, and fabrics, which is conducive to cost reduction in the fabrication and potentially installation [3]. As is well known, flexible TFSCs have significantly broaden the applications of solar cell, such as wearable solar chargers for portable electronics, and building-integrated photovoltaics on sidewalls and curved rooftops [4,5]. These factors play an important role for TFSCs in cementing its rightful place next to silicon wafer-based panels. However, currently, various thin film solar cells based on GaAs, $In_xGa_{1-x}N$, CdTe, and $CuInGaSe_2$ are facing serious obstacles, stemming from rapidly increasing raw material cost, low crustal reserve of In, Se, Te, and toxicity of As and Cd [1,2]. In addition, these photovoltaic absorber materials need to be deposited or recrystallized at temperatures at least above 400°C for constructing high-quality solar cells. Thus, they usually were deposited onto substrates with higher temperature tolerance [3,6–8]. Hence, new-type photovoltaic absorber materials, with its low-temperature fabrication process, need to be exploited to meet the aforementioned demands for TFSCs.

Ternary Zn-IV-N_2 semiconductors with IV = Sn, Ge, or Si are expected to exhibit noticeable optical properties similar to those of the well-known III-nitrides (III = In, Ga, Al), with direct band gaps ranging from the ultraviolet to infrared [9–12]. Among them, $In_xGa_{1-x}N$ and $ZnSnN_2$ are of great potential as photovoltaic absorber layers [13–15]. Compared to the rare In element, the Sn and Zn element content in the Earth's crust is 100 and 1000 times larger, respectively [14,15]. In addition, recycling infrastructure for Zn and Sn already exists [16,17]. Hence, $ZnSnN_2$, with a theoretical direct bandgap matching the AM1.5 solar spectrum and the benefit of being comprised of earth-abundant and nontoxic elements, is a good alternative utilized in the high-efficient photovoltaic absorber layer [18–20].

In comparison with the well-studied $In_xGa_{1-x}N$, however, $ZnSnN_2$ has not been investigated intensively. In recent years, polycrystalline $ZnSnN_2$ films were synthesized on monocrystalline substrates (such as sapphire, GaN, and YSZ) by plasma-assisted vapor-liquid-solid technique [21], RF sputter deposition [22], or molecular beam epitaxy [23]. The optical direct bandgap of the $ZnSnN_2$ films were determined to be around 2 eV (1.7 eV [21], 2.0 eV [22], and 2.12 eV [23]). Nevertheless, there are fewer reports on the other basic optical parameters (including the absorption coefficient [22], refractive index, and extinction coefficient) of $ZnSnN_2$ thin films. On one hand, the absorption coefficient spectrum is capable of providing an intuitive judgment on the capability of the solar radiation absorption. On the other, the refraction index and extinction coefficient are two essential parameters required in the design of optoelectronic devices.

In this work, polycrystalline $ZnSnN_2$ thin films were successfully obtained at room temperature both on quartz and flexible PET (polyethylene terephthalate) substrates. The basic optical parameters of the $ZnSnN_2$ thin films on quartz were accurately determined by the spectroscopic ellipsometry method, demonstrating that the $ZnSnN_2$ thin films possess a high absorption coefficient in the range of the solar spectrum.

$ZnSnN_2$ thin films were prepared onto quartz and PET substrates by DC magnetron sputtering at room temperature from a $Zn_{0.75}Sn_{0.25}$ alloy target. The substrates were sequentially cleaned in acetone, alcohol, and deionized water by ultrasonic method, then dried in pure nitrogen flow. Prior to deposition, the chamber was evacuated

below 6×10^{-4} Pa. As the sputtering gas, the nitrogen (5 N in purity) was imported into the chamber, and the flow rate was adjusted to be 10 sccm (standard-state cubic centimeter per minute). During the deposition, the working pressure and DC power were maintained at 1.2 Pa and 240 W, respectively. The sputtering time was 15 min. After deposition, some $ZnSnN_2$/quartz samples were annealed in a N_2 ambient at 300°C or 400°C for 3 h. The electrical properties were characterized by Hall measurement (ACCENT, HL5500). All the films display n-type semiconductor characteristics. The electron concentration decreases from 1.6×10^{18} to 2.3×10^{17} cm^{-3}, and the Hall mobility decreases from 3.98 to 1.86 $cm^2 V^{-1} s^{-1}$ as the annealing temperature increases.

Figure 1(a) presents x-ray diffraction (XRD) patterns of the $ZnSnN_2$/quartz samples using a multipurpose x-ray diffractometer (Bruker, D8 Advance) working with Cu-K_α radiation. A powder diffraction spectrum simulation result by using the orthorhombic lattice of a reported. GGA model is also illustrated as a control [9]. Three distinct peaks in the low 2θ (<40°) region are observed for the as-deposited (as-dep.) $ZnSnN_2$ film, revealing its polycrystalline nature. With increasing the annealing temperature, these three peaks get sharper, and four additional peaks in the high (>40°) 2θ region become discriminated, indicating the enhancement in the order degree. The obvious seven peaks locate at 30.6°, 33.1°, 35.0°, 45.7°, 54.2°, 59.8°, and 65.3°, respectively,

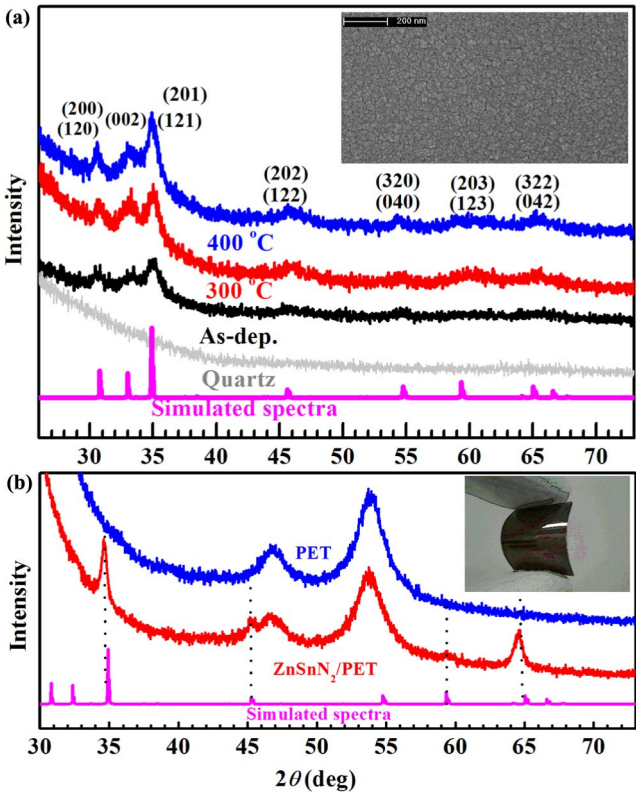

Fig. 1. (a) XRD patterns of the $ZnSnN_2$ films on quartz and calculated powder diffraction spectrum of $ZnSnN_2$. The inset shows a SEM image of the as-dep. film on quartz. (b) XRD patterns of the $ZnSnN_2$ film on flexible PET substrate. The inset shows the digital photograph of a $ZnSnN_2$ film on PET.

Table 1. Comparisons of the Experimentally Determined Lattice Parameters in this Study with Calculated Lattice Parameters from Ref. [9] and Experimentally Determined Lattice Parameters from Ref. [22]

	Calculated [9] (Å)	Experimental (Å)	Ref. [22] (Å)
a	5.80	5.853 ± 0.009	5.842 ± 0.007
b	6.70	6.741 ± 0.014	6.753 ± 0.006
c	5.53	5.498 ± 0.012	5.462 ± 0.003

matching well with the simulation result in Fig. 1(a). In addition, the fitted orthorhombic lattice parameters are also in accordance with the reported values in Ref. [22], as listed in Table 1. The average grain size [estimated by the Scherrer formula from the (201) peak] is 5.8, 6.9 and 7.5 nm for the as-dep., 300°C- and 400°C-annealed films, respectively. The small variation in crystallinity leads to slight changes in surface morphology. The insert of Fig. 1(a) shows the scanning electron microscope (SEM, Hitachi S-4800) image of the as-dep. $ZnSnN_2$ film on quartz, featuring compact, homogeneous, and smooth in nature. Figure 1(b) depicts XRD pattern of the as-dep. $ZnSnN_2$ film on PET substrate (the inset shows the digital photograph of the specimen). In the pattern, four peaks assigned to the $ZnSnN_2$ are clearly observed at 34.6°, 45.3°, 59.3°, and 64.5°, respectively. Compared to the films on quartz, these peaks are shifted toward lower angles, and meanwhile their intensity becomes stronger indicating better crystallinity, which is believed to be due to the different film/substrate strain.

The optical properties of the $ZnSnN_2$ films on quartz were characterized by a variable angle spectroscopic ellipsometer (Woollam Co.) in a photon energy ($h\nu$) range of 0.73–6.20 eV. The ellipsometric angle ψ and phase difference Δ were recorded at incidence angles of 55, 65, and 75°, respectively. A three-phase model consisting of quartz substrate/$ZnSnN_2$ film/surface rough layer (50% $ZnSnN_2$ + 50% void) was proposed to represent the sample. The Tauc–Lorentz (TL) dispersion function, as a generic model generally used for crystal semiconductor materials, was employed to determine the dielectric function of the $ZnSnN_2$ films, as shown in follows:

$$\varepsilon_2(E) = \begin{cases} \frac{AE_0C(E-E_g)^2}{(E^2-E_0^2)^2+C^2E^2}\frac{1}{E}, & (E > E_g) \\ 0, & (E \le E_g) \end{cases} \quad (1)$$

$$\varepsilon_1(E) = \varepsilon_\infty + \frac{2}{\pi}P\int_{E_g}^{\infty}\frac{\xi\varepsilon_2(\xi)}{\xi^2 - E^2}\mathrm{d}\xi, \quad (2)$$

where A is the amplitude, E_0 the peak transition energy, C the broadening term, and E_g the band gap [24]. Double TL dispersion functions were applied to fit the ellipsometry spectra in the present work. The details in the layer thicknesses and the TL parameters obtained from the data fitting are summarized in Table 2. The fitting quality was assessed on the basis of the mean-squared error (MSE) function. The MSE values are less than 5 for all the fitting, indicating that all fits are reasonable and acceptable (Generally, the fitting quality is acceptable

Table 2. Compilation of the Fitted Results for the $ZnSnN_2$/Quartz Samples Using Double Tauc–Lorentz Dispersion Function[a]

Sample	t_f	t_r	A_1	E_{g1}	E_{01}	C_1	A_2	E_{g2}	E_{02}	C_2	MSE	n
as-dep.	856.3	10.8	32.35	2.66	1.28	3.31	105.7	2.38	6.70	13.44	3.85	2.41
300°C	856.9	14.4	34.39	2.66	1.22	3.31	163.9	2.65	8.49	13.57	4.15	2.23
400°C	857.2	16.6	41.23	2.66	1.23	3.31	149.7	2.88	9.87	16.55	4.19	2.20

[a] t_f and t_r are the thicknesses of $ZnSnN_2$ film, surface rough layer with units of nanometers, respectively. MSE is mean-square error. The n values at $\lambda = 550$ nm are also listed.

only if the MSE value is less than 10). Moreover, we compare between the experimental and fitted spectroscopic spectra of the ellipsometric angle ψ and phase difference Δ for the 400°C-annealed $ZnSnN_2$ film with the biggest MSE. As shown in Fig. 2, a good superposition between the experimental and fitting spectra is observed over the studied range, meaning that the double TL dispersion function works well. Therefore, the optical parameters of the $ZnSnN_2$ films on quartz could be precisely determined by the best-fitted results.

The extracted optical constants n and k for the as-dep. and annealed $ZnSnN_2$ films are illustrated as a function of wavelength in Fig. 3(a). The refractive index decreases apparently with increasing the annealing temperature. For example, the refractive index at the wavelength $\lambda = 550$ nm is 2.41 for the as-dep. film, while the index is reduced to be 2.20 for the 400°C-annealed one, as listed in Table 2. The extinction coefficient also decreases as the annealing temperature increases, which is more evident in the short-wavelength region. It had been reported that the variations of the n and k with the annealing temperature are closely coupling with the type of ambient gas and the material itself, [25–28]. The changes in crystallinity, surface morphology, composition, or/and crystal structure may account for the n/k variations. For our case, however, further investigation is necessary to understand the variation trend of both the parameters of the $ZnSnN_2$ films.

Based on the optical absorption spectra, the nature of optical transition can be determined. In our study, the absorption coefficient α is obtained via $\alpha = 4\pi k/\lambda$. Since $ZnSnN_2$ has a direct bandgap, the inter-band absorption can be expressed by the equation [29]

$$(\alpha h\upsilon)^2 \propto h\upsilon - E_g. \tag{3}$$

The variation of $(\alpha h\upsilon)^2$ on $h\upsilon$ for the $ZnSnN_2$ films is depicted in Fig. 3(b). The band gap E_g is obtained from the energy intercept by extrapolating the linear portion of $(\alpha h\upsilon)^2$ versus $h\upsilon$ to $\alpha = 0$. For the as-dep. $ZnSnN_2$ films and the films annealed at 300°C and 400°C, the bandgap is estimated to be 1.82 eV [20], 1.92 eV [21], and 1.95 eV [22], respectively, in a good agreement with the previously reported results [21–23]. The inset of Fig. 3(b) shows the transmittance spectra of the films measured by spectroscopic ellipsometry. All the films illustrate a slight difference in the transmittance at long wavelength (>900 nm), whereas the band edge shifts gradually to the shorter wavelengths as the annealing temperature increased, which corresponds to the blue-shift of the band gaps.

High absorption coefficient in the range of the solar spectrum is one essential factor for photovoltaic conversion. Figure 4 shows the α versus λ spectrum for the as-dep. $ZnSnN_2$ film. The absorption coefficient of some other typical photovoltaic film materials and the AM1.5 solar spectrum are also plotted together for comparison. The absorption coefficient of the $ZnSnN_2$ film is as high as 10^4 cm^{-1} at $\lambda = 845$ nm ($h\upsilon = 1.48$ eV), and its absorption spans over the most region of the solar radiation

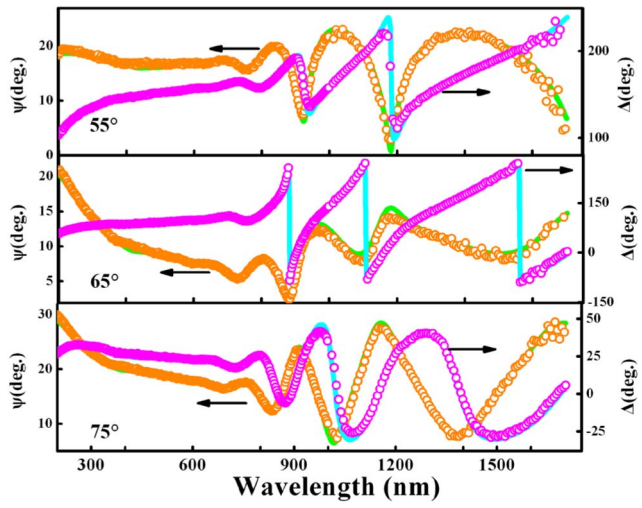

Fig. 2. Experimental (symbols) and fitted (solid curves) ψ and Δ of the $ZnSnN_2$ film annealed at 400°C.

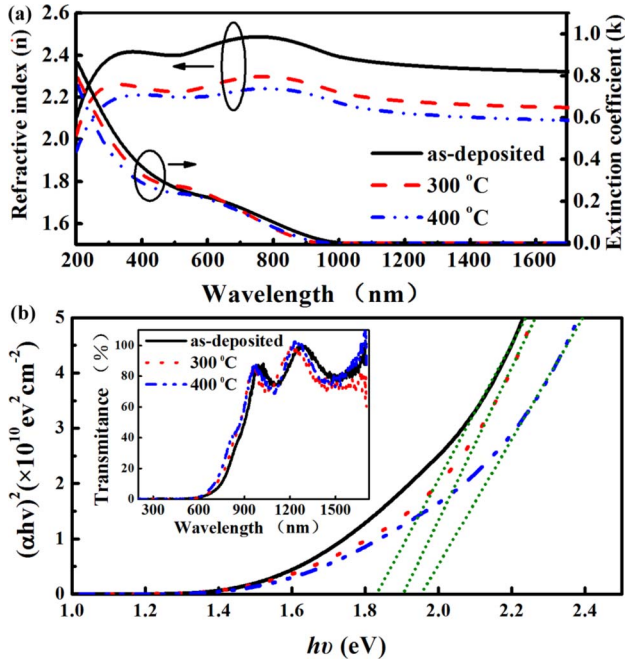

Fig. 3. (a) Refractive index and extinction coefficient spectra and (b) plots of $(\alpha h\upsilon)^2$ versus $h\upsilon$ of the $ZnSnN_2$ films on quartz. The inset shows the transmittance spectra of the films.

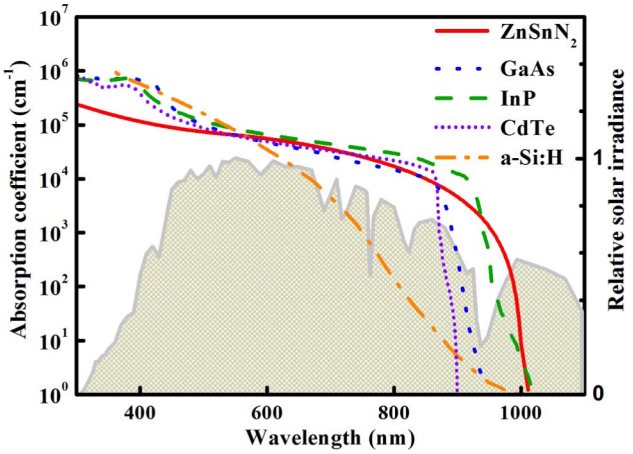

Fig. 4. Plots of the AM1.5 solar spectrum and the absorption coefficient versus light wavelength for $ZnSnN_2$, GaAs, InP, CdTe, and a-Si:H.

spectrum, ranging from the ultraviolet through visible light and into the near-infrared. Correspondingly, the α of InP, CdTe, GaAs and a-H:Si reaches to 10^4 cm^{-1} at $\lambda =$ 914 nm ($h\upsilon = 1.35$ eV), $\lambda = 865$ nm ($h\upsilon = 1.43$ eV), $\lambda =$ 850 nm ($h\upsilon = 1.46$ eV), and $\lambda = 648$ nm ($h\upsilon = 1.86$ eV), respectively. It is suggested that the useful absorption range of the $ZnSnN_2$ is wider than that of the a-H:Si, and comparable to those of the InP, CdTe, and GaAs.

In conclusion, we fabricated polycrystalline *n*-type $ZnSnN_2$ films and investigated their optical properties in detail. The influence of annealing temperature on the refraction index, extinction coefficient, and bandgap were examined. Moreover, it is revealed that the useful absorption range of the $ZnSnN_2$ is superior to that of the a-H:Si and comparable to those of the InP, CdTe, and GaAs. These results verify that $ZnSnN_2$ is a promising material for photovoltaic applications.

This work is supported by the Chinese National Program on Key Basic Research Project (2012CB933003), and the National Natural Science Foundation of China (Grant Nos. 61274095 and 61474126).

References

1. S. Das and K. C. Mandal, Mater. Res. Bull. **57**, 135 (2014).
2. P. T. Erslev, M. R. Young, J. V. Li, S. C. Siah, R. Chakraborty, H. Du, R. J. Lad, T. Buonassisi, and G. Teeter, Sol. Energy Mater. Sol. Cells **129**, 124 (2014).
3. C. H. Lee, D. R. Kim, and X. Zheng, ACS Nano **8**, 8746 (2014).
4. M. B. Schubert and J. H. Werner, Mater. Today **9**(6), 42 (2006).
5. M. Pagliaro, R. Ciriminna, and G. Palmisano, ChemSusChem. **1**, 880 (2008).
6. J. Haarstrich, H. Metzner, M. Oertel, C. Ronning, T. Rissom, C. A. Kaufmann, T. Unold, H. W. Schock, J. Windeln, W. Mannstadt, and E. Rudigier-Voigtd, Sol. Energy Mater. Sol. Cells **95**, 1028 (2011).
7. S. S. Chu, T. L. Chu, and Y. X. Han, J. Appl. Phys. **60**, 811 (1986).
8. E. Matioli, C. Neufeld, M. Iza, S. C. Cruz, A. A. Al-Heji, X. Chen, and C. Weisbuch, Appl. Phys. Lett. **98**, 021102 (2011).
9. A. Punya, W. R. Lambrecht, and M. V. Schilfgaarde, Phys. Rev. B **84**, 165204 (2011).
10. T. Endo, Y. Sato, H. Takizawa, and M. Shimada, J. Mater. Sci. Lett. **11**, 424 (1992).
11. J. E. Northrup, C. L. Chua, Z. Yang, T. Wunderer, M. Kneissl, N. M. Johnson, and T. Kolbe, Appl. Phys. Lett. **100**, 021101 (2012).
12. J. Wu, W. Walukiewicz, W. Shan, K. M. Yu, J. W. Ager, S. X. Li, and W. J. Schaff, J. Appl. Phys. **94**, 4457 (2003).
13. N. Feldberg, J. D. Aldous, P. A. Stampe, R. J. Kennedy, T. D. Veal, and S. M. Durbin, J. Electron. Mater. **43**, 884 (2014).
14. N. Duxbury, U. Bangert, P. Dawson, E. J. Thrush, W. V. Stricht, K. Jacobs, and I. Moerman, Appl. Phys. Lett. **76**, 1600 (2000).
15. Z. Liliental-Weber, D. N. Zakharov, M. Y. Kin, J. W. Ager, W. Walukiewicz, E. E. Haller, and W. J. Schaff, J. Electron Microsc. **54**, 243 (2005).
16. A. C. Tolcin, "Mineral commodity summaries" (U.S. Geological Survey, 2013), pp. 188–189, report online.
17. J. F. Carlin, "Mineral commodity summaries" (U.S. Geological Survey, 2013), pp. 170–171, report online.
18. N. Feldberg, B. Keen, J. D. Aldous, D. O. Scanlon, P. A. Stampe, R. J. Kennedy, R. J. Reeves, T. D. Veal, and S. M. Durbin, "$ZnSnN^2$: A new earth-abundant element semiconductor for solar cells," in *Proc. of the 38th IEEE Photovoltaic Specialists Conference* (IEEE, 2012), p. 2524.
19. P. Nrang, S. Chen, N. C. Coronel, S. Gul, J. Yano, L. W. Wang, and H. A. Atwater, Adv. Mater. **26**, 1235 (2014).
20. A. Punya and W. R. L. Lambrecht, Phys. Rev. B **88**, 075302 (2013).
21. L. Lahourcade, N. C. Coronel, K. T. Delaney, S. K. Shukla, N. A. Spaldin, and H. A. Atwater, Adv. Mater. **25**, 2562 (2013).
22. P. C. Quayle, K. He, J. Shan, and K. Kash, MRS Communications **3**, 135 (2013).
23. N. Feldberg, J. D. Aldous, W. M. Linhart, L. J. Phillips, K. Durose, P. A. Stampe, and S. M. Durbin, Appl. Phys. Lett. **103**, 042109 (2013).
24. L. Y. Liang, Z. M. Liu, H. T. Cao, Y. Y. Shi, X. L. Sun, Z. Yu, A. H. Chen, H. Z. Zhang, and Y. Q. Fang, ACS Appl. Mater. Inter. **2**, 1565 (2010).
25. S. D'Elia, N. Scaramuzza, F. Ciuchi, C. Versace, G. Strangi, and R. Bartolino, Appl. Surf. Sci. **255**, 7203 (2009).
26. S. Baco, A. Chik, and F. M. Yassin, J. Sci. Technol. **4**, 61 (2012).
27. M. Mosaddeq-ur-Rahman, G. L. Yu, T. Soga, T. Jimbo, H. Ebisu, and M. Umeno, J. Appl. Phys. **88**, 4634 (2000).
28. M. I. Abd-Elrahman, A. Y. Abdel-Latief, R. M. Khafagy, N. Younis, and M. M. Hafiz, Spectrochim. Acta. A **137**, 29 (2015).
29. F. Wooten, *Optical Properties of Solids* (Academic, 1972).